Loss Minimization Control Based on Bivariate Extreme Value Theory for PMSMs

Zhuang Liu, Kun Mao, *Member, IEEE*, Xusheng Lei, Shiqiang Zheng, *Member, IEEE*, and Haifeng Zhang

***Abstract*—As considering both copper loss and iron loss, the loss minimization control (LMC) method could help permanent magnet synchronous motors (PMSMs) get higher efficiency compared with the traditional maximum torque per ampere control method. Unfortunately, it suffers from approximate models and the electromagnetic torque, which is hard to get precisely. To overcome these shortcomings and further improve efficiency, this article proposes an improved LMC method based on bivariate extreme value theory for PMSMs. First of all, based on the equivalent model of PMSM considering both copper loss and iron loss, the electrical loss of the PMSM is transformed into a function of the *d*-*q*-axis currents. Then, according to the bivariate extreme value theory, the optimal *d*-*q*-axis currents without the torque constraint are obtained. On this basis, the optimal *d*-axis active current model is derived, while the *q*-axis active current is obtained by the speed controller. After that a current regulator with the feedforward decoupling control of iron loss currents is designed to realize the LMC strategy with implicit torque constraint. At last, implementing comparative experiments with $i_{\mathrm{d}} = 0$ control and traditional LMC method, the improved LMC strategy can increase the efficiency of PMSMs significantly, which verifies its effectiveness.**

***Index Terms*—Bivariate extreme value theory, copper loss, feedforward decoupling control, iron loss, loss minimization control (LMC), permanent magnet synchronous motor (PMSM).**

I. Introduction

In THE last decades, permanent magnet synchronous motor (PMSM) systems have been widely used in the field of electric vehicles [1], [2], [3] because of their simple structure, high torque-current ratio, high power density, and low power loss [4], [5], [6]. It is crucial to improve the efficiency of PMSM systems for longer battery life and driving distance. Optimizing the structure and material design of PMSM [7], [8], [9], [10] is not the only way to improve the efficiency of the drives. Different kinds of high efficiency control methods can also be used to increase their performance. Typically, the field-oriented control (FOC) [11], which simplifies controller design, like the $i_{\mathrm{d}} = 0$ strategy, is used for PMSM systems. But in this way, the air-gap flux is uncontrollable so that the efficiency of the PMSM cannot be optimized. To solve this problem, researchers have proposed a variety of loss minimization control (LMC) methods, such as maximum torque per ampere (MTPA) control, online search control (SC), and LMC [12], [13], [14], [15], [16].

The MTPA control method minimizes motor current while maintaining constant motor torque [17], [18], [19]. Despite this, the *d*-*q*-axis currents are derived from the torque equation, which ignores iron loss. Therefore, the MTPA control can achieve the minimum copper loss merely, which is a local optimal solution. The SC method is also referred to as minimum input power control. The stator current is regulated continuously to maximize the operation efficiency [20], [21], [22]. This method optimizes the entire drive system including the motor and inverter, so that it can achieve a global optimization. Since the SC method has a low response speed, it can only decrease motor losses in steady state, which greatly limits its applicability. Comprehensively considering the iron loss and copper loss, the LMC method can realize a global optimization of motor losses [23], [24], [25]. It has a great potential for application because of its high response speed and high reliability.

In traditional LMC method, the iron loss and copper loss of PMSMs are modeled by *d*-*q*-axis active currents. Depending on the unary extremum theory, a mathematical model of optimal current can be obtained. The loss model, which is complicated, is a quartic function of the *d*-axis active current, so the ideal *d*-axis active current must be calculated at first. Then, through complex transformations, the model of the ideal *d*-axis current can be obtained. Unfortunately, to eliminate the *q*-axis active current, the electromagnetic torque is introduced into the loss model based on the electromagnetic torque function of the PMSM in the above-mentioned process [23], [24], [25].

By the equivalent transformation of the controlled variable, Hang [23] carries out a novel LMC method that improves the optimal current models. But the electromagnetic torque which the optimal current models included is introduced by the speed PI controller so that its accuracy is limited by the measurement noise of the sensor and the phase delay of the controller. Uddin [24] proposed a direct torque and flux control based LMC method for PMSMs. It reduces the electrical loss of PMSMs by optimizing the air-gap flux. Nevertheless, the observers for electromagnetic torque and flux are essential in this method. Moreover, a loss model based nonlinear controller (LMNC) is designed by him to achieve an efficiency improvement and a great dynamic performance of PMSMs in [25]. To cope with the

Manuscript received 15 November 2022; revised 18 April 2023 and 18 June 2023; accepted 14 August 2023. Date of publication 22 August 2023; date of current version 22 December 2023. This work was supported by the National Natural Science Foundation of China under Grants 61873016 and 62225301. Recommended for publication by Associate Editor K. Akatsu. *(Corresponding authors: Kun Mao; Haifeng Zhang.)*

The authors are with the School of Instrumentation Science and Opto-electronics Engineering, Beihang University, Beijing 100191, China (e-mail: lz_liuzhuang@buaa.edu.cn; kunmao@buaa.edu.cn; yushangtianxia@163.com; zhengshiqiang@buaa.edu.cn; zhanghaifeng@buaa.edu.cn).

Color versions of one or more figures in this article are available at https://doi.org/10.1109/TPEL.2023.3307237.

Digital Object Identifier 10.1109/TPEL.2023.3307237

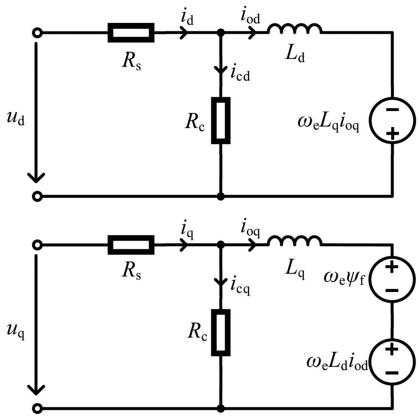

Fig. 1. Equivalent model of the PMSM with iron loss resistance.

parameter uncertainties, an online estimation of the motor mechanical parameters such as the friction coefficient and the load torque is introduced. However, the LMNC, which is composed of nonlinear controller, loss minimization, and online parameter estimation algorithm, is a little complicated.

In most applications, the electromagnetic torque cannot be obtained accurately, which is essential to be measured by torque sensors or estimated by state observers. As a result, the traditional LMC strategy is complex and the accuracy is limited.

The rest of this article is organized as follows. To solve the traditional LMC problems, this article proposes an improved LMC method based on the bivariate extreme value theory. In Section II, the equivalent model of PMSMs considering copper loss and iron loss is presented. In Section III, the derivation of optimal currents model and the control block diagram of the improved LMC strategy are introduced. In Section IV, compared with $i_d = 0$ control and traditional LMC strategies, the experiment results indicate that the proposed LMC method can comprehensively reduce the electrical loss of the PMSM. Finally, Section V concludes this article.

II. Equivalent Model of PMSMs Considering Copper Loss and Iron Loss

In steady state, the loss of PMSMs mainly includes copper loss, iron loss, friction loss, and stray loss. The stray loss is ignored in this article because it is much lower than other kinds of power loss. Meanwhile, related to speed, the friction loss cannot be reduced by control strategies. Hence, it is rational to decrease the electrical loss which includes copper loss and iron loss.

Considering the copper loss and iron loss, Fig. 1 shows the equivalent model [23], [24], [25] of PMSMs. In Fig. 1, u_d and u_q are d-q-axis voltages, respectively, i_d and i_q are d-q-axis currents, respectively, i_{cd} and i_{cq} are d-q-axis iron loss currents, respectively, i_{od} and i_{oq} are d-q-axis active currents, respectively, R_s and R_c are stator phase resistance and iron loss resistance, respectively. The iron loss resistance R_c of PMSM can be estimated by approximate calculation [26], [27], [28] or finite-element method [29], [30]. In this article, it is obtained by approximate calculation scheme proposed in [26]. L_d and L_q are d-q-axis inductances, respectively, ψ_f is the permanent magnet flux linkage, and ω_e is the electric angular velocity of the motor.

According to the equivalent circuit, in the synchronous reference frame, the voltage equation of the PMSM is expressed as follows:

$$\begin{cases} u_d = R_s i_d + L_d \frac{di_{od}}{dt} - \omega_e L_q i_{oq} \\ u_q = R_s i_q + L_q \frac{di_{oq}}{dt} + \omega_e \left(L_d i_{od} + \psi_f\right). \end{cases} \tag{1}$$

In synchronous reference frame, the current equation of the PMSM is expressed as follows:

$$\begin{cases} i_d = i_{od} + \frac{L_d}{R_c} \frac{di_{od}}{dt} - \frac{\omega_e L_q i_{oq}}{R_c} \\ i_q = i_{oq} + \frac{L_q}{R_c} \frac{di_{oq}}{dt} + \frac{\omega_e (L_d i_{od} + \psi_f)}{R_c}. \end{cases} \tag{2}$$

When the constant amplitude is used as the constraint condition for coordinate transformation, where T_e is the electromagnetic torque of the PMSM, the torque equation is expressed as follows:

$$T_e = \frac{3}{2} p \left[\psi_f i_{oq} + \left(L_d - L_q\right) i_{od} i_{oq}\right]. \tag{3}$$

Respectively, the copper loss P_{cu}, iron loss P_{fe}, and electrical loss P_e of PMSMs are calculated as follows:

$$P_{cu} = \frac{3}{2} R_s \left(i_d^2 + i_q^2\right) \tag{4}$$

$$P_{fe} = \frac{3}{2} R_c \left(i_{cd}^2 + i_{cq}^2\right) \tag{5}$$

$$P_e = P_{fe} + P_{cu}. \tag{6}$$

III. Optimal Model and Control Block Diagram of Improved LMC Strategy

A. Conventional LMC Method

Based on the equivalent circuit shown in Fig. 1, the current equation of PMSMs under steady condition is expressed as follows:

$$\begin{cases} i_d = i_{od} + i_{cd} \\ i_q = i_{oq} + i_{cq} \\ i_{cd} = -\frac{\omega_e L_q i_{oq}}{R_c} \\ i_{cq} = \frac{\omega_e (L_d i_{od} + \psi_f)}{R_c}. \end{cases} \tag{7}$$

The conventional LMC method is based on the FOC with the superior reference of d-axis current. The control of q-axis current is consistent with the FOC method, while the d-axis current is controlled to maintain the optimal d-axis reference current. In steady state, the copper loss P_{cu}, iron loss P_{fe}, and electrical loss P_e of conventional LMC method is a function of the d-q-axis active currents i_{od}, i_{oq}. Hence, based on (7), (4)–(6) can be transformed into

$$P_{cu} = \frac{3}{2} R_s \left\{ \left(-\frac{\omega_e L_q i_{oq}}{R_c} + i_{od} \right)^2 + \left[\frac{\omega_e \left(L_d i_{od} + \psi_f\right)}{R_c} + i_{oq} \right]^2 \right\} \tag{8}$$

$$P_{fe} = \frac{3\omega_e^2}{2R_c} \left[\left(L_q i_{oq}\right)^2 + \left(L_d i_{od} + \psi_f\right)^2 \right] \tag{9}$$

$$P_{\mathrm{e}}=\frac{3}{2}R_{\mathrm{s}}\left[\left(-\frac{\omega_{\mathrm{e}}L_{\mathrm{q}}i_{\mathrm{oq}}}{R_{\mathrm{c}}}+i_{\mathrm{od}}\right)^2+\left(\frac{\omega_{\mathrm{e}}L_{\mathrm{d}}i_{\mathrm{od}}+\omega_{\mathrm{e}}\psi_{\mathrm{f}}}{R_{\mathrm{c}}}+i_{\mathrm{oq}}\right)^2\right]+\frac{3\omega_{\mathrm{e}}^2}{2R_{\mathrm{c}}}\left[\left(L_{\mathrm{q}}i_{\mathrm{oq}}\right)^2+\left(L_{\mathrm{d}}i_{\mathrm{od}}+\psi_{\mathrm{f}}\right)^2\right]. \tag{10}$$

By substituting (3) into (10), the electrical loss is transformed into a function of d-axis active current i_{od}, electric angular velocity ω_{e}, and electromagnetic torque T_{e}. In steady state, both the ω_{e} and T_{e} are regarded as constant values so that the electrical loss P_{e} is only related to i_{od}. The optimal d-axis active current of minimum loss can be obtained by the unary extreme value theory as follows:

$$i_{\mathrm{od}}=-\frac{\omega_{\mathrm{e}}^2\psi_{\mathrm{f}}L_{\mathrm{d}}\left(R_{\mathrm{s}}+R_{\mathrm{c}}\right)}{R_{\mathrm{s}}R_{\mathrm{c}}^2+\left(R_{\mathrm{s}}+R_{\mathrm{c}}\right)\omega_{\mathrm{e}}^2L_{\mathrm{d}}^2}. \tag{11}$$

Combining (2) and (3), the corresponding optimal d-axis current is expressed as follows:

$$i_{\mathrm{dref}}=-\frac{\left(R_{\mathrm{s}}+R_{\mathrm{c}}\right)\psi_{\mathrm{f}}L_{\mathrm{d}}\omega_{\mathrm{e}}^2}{R_{\mathrm{s}}R_{\mathrm{c}}^2+\left(R_{\mathrm{s}}+R_{\mathrm{c}}\right)L_{\mathrm{d}}^2\omega_{\mathrm{e}}^2}-\frac{2\omega_{\mathrm{e}}L_{\mathrm{q}}T_{\mathrm{e}}\left[R_{\mathrm{s}}R_{\mathrm{c}}^2+L_{\mathrm{d}}^2\left(R_{\mathrm{s}}+R_{\mathrm{c}}\right)\omega_{\mathrm{e}}^2\right]}{3pR_{\mathrm{c}}\psi_{\mathrm{f}}\left[R_{\mathrm{s}}R_{\mathrm{c}}^2+L_{\mathrm{d}}L_{\mathrm{q}}\left(R_{\mathrm{s}}+R_{\mathrm{c}}\right)\omega_{\mathrm{e}}^2\right]}. \tag{12}$$

However, it can be seen from (3) and (10) that P_{e} is a quartic function of i_{od}, which brings about a complicated modeling process of traditional LMC method.

B. Optimal Model of Improved LMC Method

Eliminating the i_{od} and i_{oq} of (7), the d-q-axis iron loss currents are derived as follows:

$$\begin{cases} i_{\mathrm{cd}}=\frac{-\omega_{\mathrm{e}}R_{\mathrm{c}}L_{\mathrm{q}}i_{\mathrm{q}}+\omega_{\mathrm{e}}^2L_{\mathrm{d}}L_{\mathrm{q}}i_{\mathrm{d}}+\omega_{\mathrm{e}}^2L_{\mathrm{q}}\psi_{\mathrm{f}}}{R_{\mathrm{c}}^2+L_{\mathrm{d}}L_{\mathrm{q}}\omega_{\mathrm{e}}^2} \\ i_{\mathrm{cq}}=\frac{\omega_{\mathrm{e}}(R_{\mathrm{c}}L_{\mathrm{d}}i_{\mathrm{d}}+R_{\mathrm{c}}\psi_{\mathrm{f}}+\omega_{\mathrm{e}}L_{\mathrm{d}}L_{\mathrm{q}}i_{\mathrm{q}})}{R_{\mathrm{c}}^2+L_{\mathrm{d}}L_{\mathrm{q}}\omega_{\mathrm{e}}^2}. \end{cases} \tag{13}$$

The copper loss model of the PMSM is shown in (4). Substituted (13) into (5) and (6), the iron loss and electrical loss of the PMSM are calculated as follows:

$$P_{\mathrm{fe}}=\frac{3}{2}R_{\mathrm{c}}\omega_{\mathrm{e}}^2\left(\frac{-R_{\mathrm{c}}L_{\mathrm{q}}i_{\mathrm{q}}+\omega_{\mathrm{e}}L_{\mathrm{d}}L_{\mathrm{q}}i_{\mathrm{d}}+\omega_{\mathrm{e}}L_{\mathrm{q}}\psi_{\mathrm{f}}}{R_{\mathrm{c}}^2+L_{\mathrm{d}}L_{\mathrm{q}}\omega_{\mathrm{e}}^2}\right)^2+\frac{3}{2}R_{\mathrm{c}}\omega_{\mathrm{e}}^2\left(\frac{R_{\mathrm{c}}L_{\mathrm{d}}i_{\mathrm{d}}+R_{\mathrm{c}}\psi_{\mathrm{f}}+\omega_{\mathrm{e}}L_{\mathrm{d}}L_{\mathrm{q}}i_{\mathrm{q}}}{R_{\mathrm{c}}^2+L_{\mathrm{d}}L_{\mathrm{q}}\omega_{\mathrm{e}}^2}\right)^2 \tag{14}$$

$$P_{\mathrm{e}}=\frac{3}{2}R_{\mathrm{s}}\left(i_{\mathrm{d}}^2+i_{\mathrm{q}}^2\right)+\frac{3R_{\mathrm{c}}\omega_{\mathrm{e}}^2\left(-R_{\mathrm{c}}L_{\mathrm{q}}i_{\mathrm{q}}+\omega_{\mathrm{e}}L_{\mathrm{d}}L_{\mathrm{q}}i_{\mathrm{d}}+\omega_{\mathrm{e}}L_{\mathrm{q}}\psi_{\mathrm{f}}\right)^2}{2\left(R_{\mathrm{c}}^2+L_{\mathrm{d}}L_{\mathrm{q}}\omega_{\mathrm{e}}^2\right)^2}+\frac{3R_{\mathrm{c}}\omega_{\mathrm{e}}^2\left(R_{\mathrm{c}}L_{\mathrm{d}}i_{\mathrm{d}}+R_{\mathrm{c}}\psi_{\mathrm{f}}+\omega_{\mathrm{e}}L_{\mathrm{d}}L_{\mathrm{q}}i_{\mathrm{q}}\right)^2}{2\left(R_{\mathrm{c}}^2+L_{\mathrm{d}}L_{\mathrm{q}}\omega_{\mathrm{e}}^2\right)^2}. \tag{15}$$

In (15), P_{e} is a function of i_{d} and i_{q}. According to the theory of bivariate extreme value theory, the possible extreme point (i_{dref}, i_{qref}) without the torque constraint is the solution of

$$\begin{cases} \frac{\partial P_{\mathrm{e}}}{\partial i_{\mathrm{d}}}=0 \\ \frac{\partial P_{\mathrm{e}}}{\partial i_{\mathrm{q}}}=0. \end{cases} \tag{16}$$

The possible optimal d-q-axis currents i_{dref} and i_{qref} are calculated as follows:

$$\begin{cases} i_{\mathrm{dref}}=\frac{-L_{\mathrm{d}}R_{\mathrm{c}}\psi_{\mathrm{f}}\omega_{\mathrm{e}}^2\left[\left(R_{\mathrm{c}}+R_{\mathrm{s}}\right)L_{\mathrm{q}}^2\omega_{\mathrm{e}}^4+R_{\mathrm{c}}^2R_{\mathrm{s}}\right]}{a\omega_{\mathrm{e}}^4+b\omega_{\mathrm{e}}^2+c} \\ i_{\mathrm{qref}}=\frac{L_{\mathrm{q}}\left(L_{\mathrm{q}}-L_{\mathrm{d}}\right)R_{\mathrm{c}}^2R_{\mathrm{s}}\psi_{\mathrm{f}}\omega_{\mathrm{e}}^3}{a\omega_{\mathrm{e}}^4+b\omega_{\mathrm{e}}^2+c}. \end{cases} \tag{17}$$

Where a, b, and c represent the coefficient of the possible optimal d-q-axis currents, respectively. These coefficients are constant in steady state, which are expressed as follows:

$$\begin{cases} a=\left[L_{\mathrm{d}}L_{\mathrm{q}}\left(R_{\mathrm{c}}+R_{\mathrm{s}}\right)\right]^2 \\ b=R_{\mathrm{c}}^2R_{\mathrm{s}}\left[\left(L_{\mathrm{d}}^2+L_{\mathrm{q}}^2\right)R_{\mathrm{c}}+2L_{\mathrm{d}}L_{\mathrm{q}}R_{\mathrm{s}}\right] \\ c=R_{\mathrm{c}}^4R_{\mathrm{s}}^2. \end{cases} \tag{18}$$

According to (15), the variables A, B, and C are defined as follows:

$$\begin{cases} A=\frac{\partial^2P_{\mathrm{e}}}{\partial i_{\mathrm{d}}^2}=3\left[R_{\mathrm{s}}+\frac{R_{\mathrm{c}}L_{\mathrm{d}}^2\omega_{\mathrm{e}}^2\left(R_{\mathrm{c}}^2+L_{\mathrm{q}}^2\omega_{\mathrm{e}}^2\right)}{\left(R_{\mathrm{c}}^2+L_{\mathrm{d}}L_{\mathrm{q}}\omega_{\mathrm{e}}^2\right)^2}\right] \\ B=\frac{\partial^2P_{\mathrm{e}}}{\partial i_{\mathrm{d}}\partial i_{\mathrm{q}}}=\frac{3L_{\mathrm{d}}L_{\mathrm{q}}\left(L_{\mathrm{d}}-L_{\mathrm{q}}\right)R_{\mathrm{c}}^2\omega_{\mathrm{e}}^3}{\left(R_{\mathrm{c}}^2+L_{\mathrm{d}}L_{\mathrm{q}}\omega_{\mathrm{e}}^2\right)^2} \\ C=\frac{\partial^2P_{\mathrm{e}}}{\partial i_{\mathrm{q}}^2}=3\left[R_{\mathrm{s}}+\frac{R_{\mathrm{c}}L_{\mathrm{q}}^2\omega_{\mathrm{e}}^2\left(R_{\mathrm{c}}^2+L_{\mathrm{d}}^2\omega_{\mathrm{e}}^2\right)}{\left(R_{\mathrm{c}}^2+L_{\mathrm{d}}L_{\mathrm{q}}\omega_{\mathrm{e}}^2\right)^2}\right]. \end{cases} \tag{19}$$

The $AC-B^2$ is derived as follows:

$$AC-B^2=\frac{9\left(a\omega_{\mathrm{e}}^4+b\omega_{\mathrm{e}}^2+c\right)}{\left(R_{\mathrm{c}}^2+L_{\mathrm{d}}L_{\mathrm{q}}\omega_{\mathrm{e}}^2\right)^2}. \tag{20}$$

Since the molecules and denominators of (20) are positive, $AC-B^2>0$ can be confirmed. Hence, according to the theory of bivariate extreme value theory, the extreme value of P_{e} exists when the optimal d-q-axis currents are expressed as (17). And it can be confirmed that the extreme value is the minimum in terms of the function properties of P_{e}.

According to (7), the model of d-axis active current can be expressed by d-q-axis currents as follows:

$$i_{\mathrm{od}}=\frac{R_{\mathrm{c}}^2i_{\mathrm{d}}+\omega_{\mathrm{e}}R_{\mathrm{c}}L_{\mathrm{q}}i_{\mathrm{q}}-\omega_{\mathrm{e}}^2L_{\mathrm{q}}\psi_{\mathrm{f}}}{R_{\mathrm{c}}^2+L_{\mathrm{d}}L_{\mathrm{q}}\omega_{\mathrm{e}}^2}. \tag{21}$$

Therefore, the optimal model of d-axis active current is calculated as follows:

$$i_{\mathrm{od}}^*=\frac{-\psi_{\mathrm{f}}\omega_{\mathrm{e}}^2\left[R_{\mathrm{c}}^2R_{\mathrm{s}}\left(L_{\mathrm{d}}R_{\mathrm{c}}+L_{\mathrm{q}}R_{\mathrm{s}}\right)+L_{\mathrm{d}}L_{\mathrm{q}}^2\left(R_{\mathrm{c}}+R_{\mathrm{s}}\right)^2\omega_{\mathrm{e}}^2\right]}{a\omega_{\mathrm{e}}^4+b\omega_{\mathrm{e}}^2+c}. \tag{22}$$

C. Control Block Diagram of Improved LMC Method

Based on the equivalent model of PMSM considering both copper loss and iron loss, it can be found that d-q-axis active currents control PMSMs actually. Because of $L_{\mathrm{d}}=L_{\mathrm{q}}$, the electromagnetic torque model of surface-mounted PMSMs include no reluctance torque. Hence, their electromagnetic torque T_{e} is merely related to q-axis active current. For interior PMSMs, according to (3) based on the parameters of different rated torque motors, it can be confirmed that the d-axis active current has

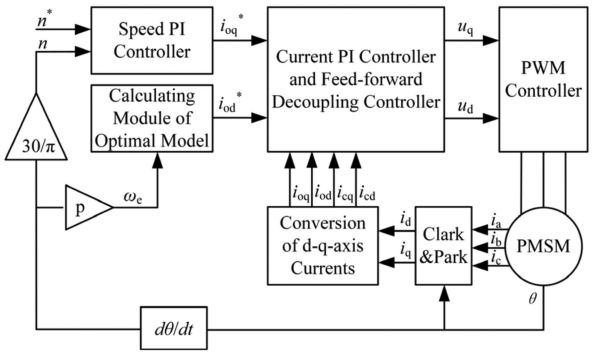

Fig. 2. Control block diagram of improved LMC strategy.

little effect on electromagnetic torque. Obviously, the influence of electromagnetic torque on the optimal d-axis active current model of PMSMs is negligible. Therefore, the optimal d-axis active current model based on the bivariate extreme value theory is used to design the control law. Meanwhile, in order to consider the torque constraint without introducing electromagnetic torque, the optimal q-axis active current is generated by the speed PI controller.

The control block diagram of the improved LMC strategy is shown in Fig. 2. The reference of optimal q-axis active current $i_{\mathrm{oq}}{}^{*}$ which implies the torque constraint is obtained through the speed PI controller with the reference speed n^{*} and the actual speed n. The actual electric angular velocity ω_{e} of the PMSM is fed back to the calculating module of optimal model, so that the reference of the d-axis active current $i_{\mathrm{od}}{}^{*}$ is obtained. The d-q-axis voltages u_{d} and u_{q} are obtained through the current PI controller and the feedforward decoupling controller. Then the pulsewidth modulation signal can be obtained by transforming u_{d} and u_{q} to drive the PMSM. Meanwhile, based on (7) and (13), the d-q-axis currents are transformed into d-q-axis active currents and d-q-axis iron loss currents. Finally, the transformed currents and position signals of the PMSM are fed back to the controller to form a closed loop.

As shown in Fig. 3, according to the equivalent model of PMSM considering copper loss and iron loss, the u_{d} and u_{q} are composed of the voltage components u_{d1} and u_{q1} generated by corresponding active currents and the voltage components u_{d2} and u_{q2} generated by corresponding iron loss currents on R_{s}, respectively. The voltage equation of those components is expressed as follows:

$$\begin{cases} u_{\mathrm{d}} = u_{\mathrm{d1}} + u_{\mathrm{d2}} \\ u_{\mathrm{q}} = u_{\mathrm{q1}} + u_{\mathrm{q2}}. \end{cases} \tag{23}$$

The specific structure of the current PI controller and the feedforward decoupling controller is shown in Fig. 4. The current controller consists of two PI regulators. According to (13), combined with the actual d-q-axis current, the d-q-axis iron loss current i_{cd} and i_{cq} can be obtained. A feedforward decoupling control based on i_{cd} and i_{cq} is designed to compensate the voltage drop caused by iron loss current on R_{s}.

In summary, according to the optimal model based on the bivariate extreme value theory and the novel design of the control

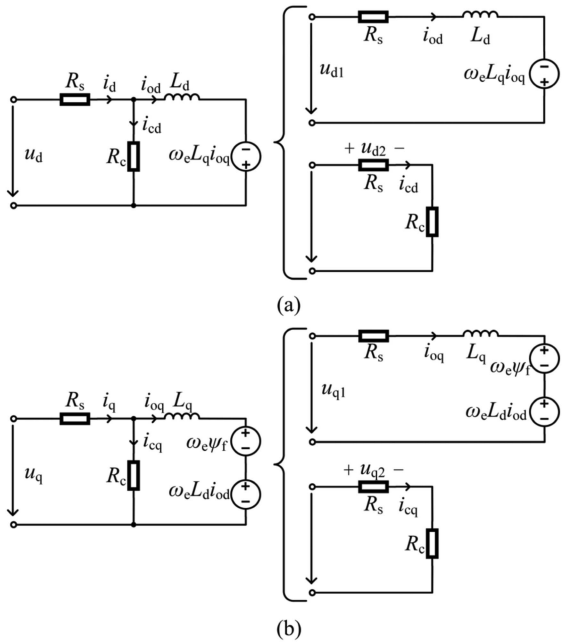

Fig. 3. Decomposition of PMSM Equivalent Model. (a) Decomposition of d-axis circuit. (b) Decomposition of q-axis circuit.

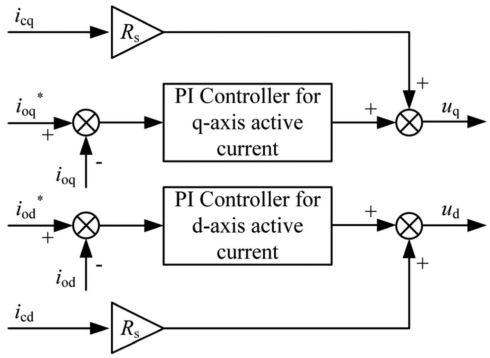

Fig. 4. Control block diagram of current controller.

block diagram with feedforward compensation, the improved LMC strategy with implicit torque constraint can be realized.

IV. Experiment Verification

To verify the effectiveness of the proposed algorithm, the comparative experiment is implemented among the $i_{\mathrm{d}} = 0$ control method (Method I), traditional LMC method (Method II), and proposed control method (Method III). The experiment platform is shown in Fig. 5. The parameters of the 380 W PMSM are shown in Table I, and the iron loss resistance therein is estimated by approximate calculation scheme proposed in [26]. The PMSM is connected to one end of the torque sensor through a coupling, and the other end is connected to the hysteresis brake by the same way. All the control strategies in the comparative experiment are implemented based on the TMS320F28069 DSP platform. The load torque provided by hysteresis brake is regulated through the controlled current source. The input power is measured by the power meter HIOKI PW3337, and the output

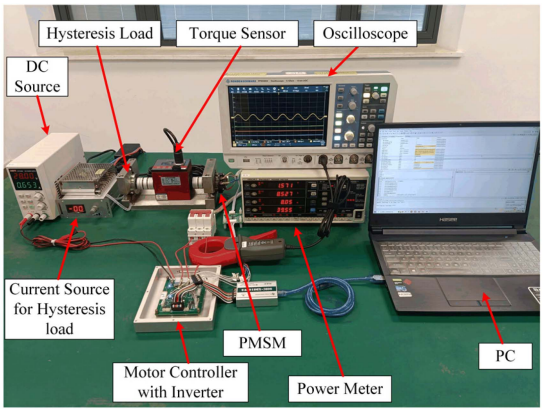

Fig. 5. Experiment platform.

TABLE I
PARAMETER OF THE INVESTIGATED PMSM

Parameter	Value	Parameter	Value
Rated power(W)	380	Rated voltage(V)	28
Rated speed(r/min)	6000	Rated torque(N·m)	0.5
d-axis inductance(H)	41.5×10^{-6}	q-axis inductance (H)	45×10^{-6}
Phase resistance(Ω)	0.048	Number of pole pairs	1
Iron loss resistance(Ω)	4.6	Permanent magnet flux linkage (Wb)	0.0166

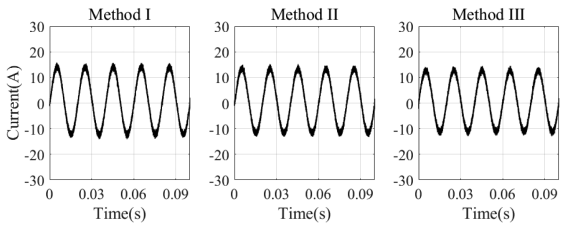

Fig. 6. Phase currents of the PMSM with the three methods.

power is measured by the torque sensor. Meanwhile, the current waveform is monitored by the oscilloscope Rohde&Schwarz RTM3004. Based on the experimental data, the different power loss can be separated. The copper loss of the PMSM is obtained from the phase resistance and the three-phase RMS current measured by PW3337. The iron loss and the friction loss of the PMSM are obtained by subtracting the output power and the copper loss from the input power.

A. Steady-State Performance

At the reference speed 3000 r/min with the load torque 0.3 N·m, the phase current waveforms, the phase current spectrums, the reference and actual waveforms of d-q-axis active currents, the torque curves and the output power curves of the PMSM are shown in Figs. 6 –11 in order. Fig. 6 shows the phase current of the PMSM with the improved LMC strategy in steady-state is similar to that of the others. While the current amplitude is 11.97 A with Method III which is lower than 12.54 A with Method II, and 13.14 A with Method I in Fig. 7. Meanwhile, the d-axis active reference current $i_{\mathrm{od}}{}^{*}$ and the actual current i_{od} of

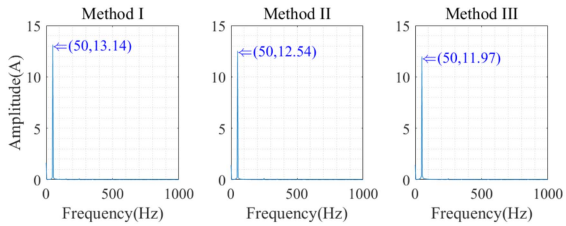

Fig. 7. Phase current spectrum of the PMSM with the three methods.

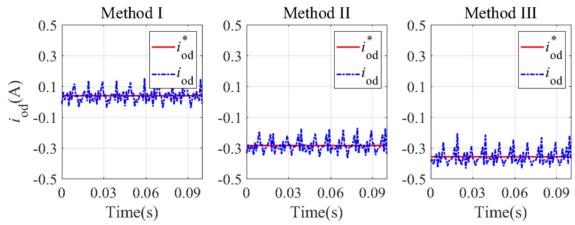

Fig. 8. d-axis active currents of the PMSM with the three methods.

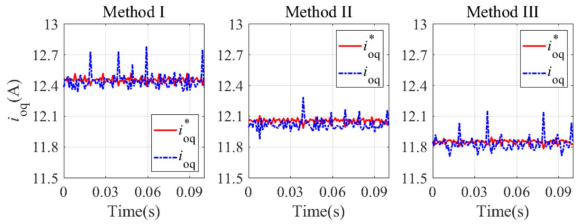

Fig. 9. q-axis active currents of the PMSM with the three methods.

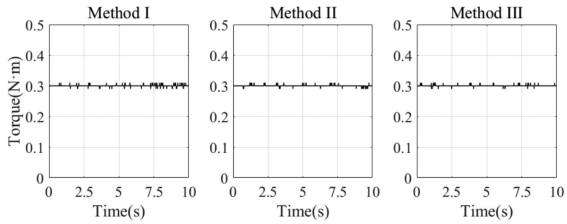

Fig. 10. Output torque curves of the PMSM with the three methods.

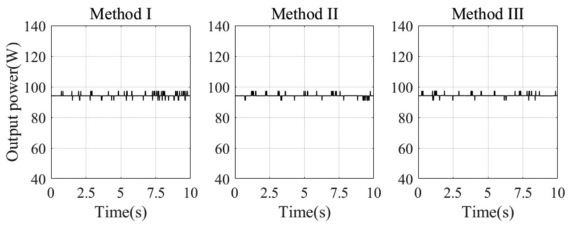

Fig. 11. Output power curves of the PMSM with the three methods.

the three methods are shown in Fig. 8. The q-axis active reference current $i_{\mathrm{oq}}{}^{*}$ and the actual current i_{oq} of the three methods are shown in Fig. 9. It can be found that the d-q-axis actual active currents of the three methods can track the reference well. In addition, the motor speed and the output torque of the PMSM

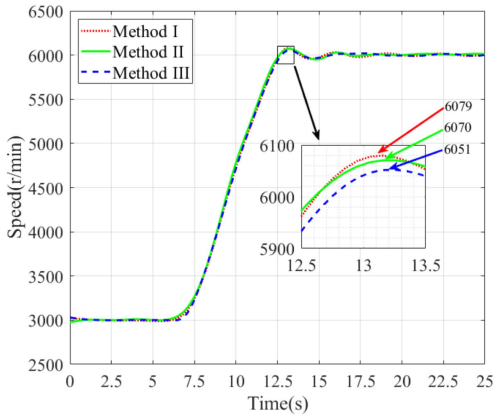

Fig. 12. Dynamic speed curves of the PMSM with the three methods.

with the three strategies can follow the reference speed and load torque well. The output power of the PMSM with the three strategies which fluctuates around 94.2 W follows the speed and torque variation. Therefore, the steady-state performance of the proposed improved LMC strategy is similar to that of Methods I and II.

B. Dynamic Performance

With the reference speed of the PMSM increased from 3000–6000 r/min at the load torque 0.3 N·m, Fig. 12 shows the speed curves of the PMSM with the three strategies have similar trace and adjusting-time. During the transient process, the peak speed of the PMSM with the proposed LMC method is 6051 r/min, which is slightly lower than 6079 r/min of Method I and 6070 r/min of Method II. It can be concluded that the dynamic performance of the proposed LMC strategy is similar to that of $i_d = 0$ control strategy and traditional LMC strategy.

C. Electrical Loss and Efficiency at Varied Operating Point

The PMSM RMS phase currents are recorded at different operating points which the speed varies from 1000 to 6000 r/min and the load torque varies from 0.1 to 0.5 N·m. Then based on the phase resistance R_s, the copper losses of the PMSM at varied operating points are obtained. The three-dimensional (3-D) figures of the copper losses based on the speed and torque with the three control methods are shown in Fig. 13. The mapping of the vertical color bars to the copper loss of the three methods is consistent. It can be seen that the copper loss with Method II is lower than that of Method I, and the copper loss with Method III is lower than that of Method II. For example, at the reference speed 6000 r/min with the load torque 0.5 N·m, the copper loss of the PMSM with Method III is 25.12 W, which is lower than 29.02 W of Method I and 26.65 W of Method II. In other words, with the comparison of Method I and Method II, the copper loss with Method III is reduced by 13.44% and 5.74%, respectively. Therefore, compared with the traditional LMC strategy, the improved LMC strategy can further reduce the copper loss of PMSMs. Moreover, the copper loss of the

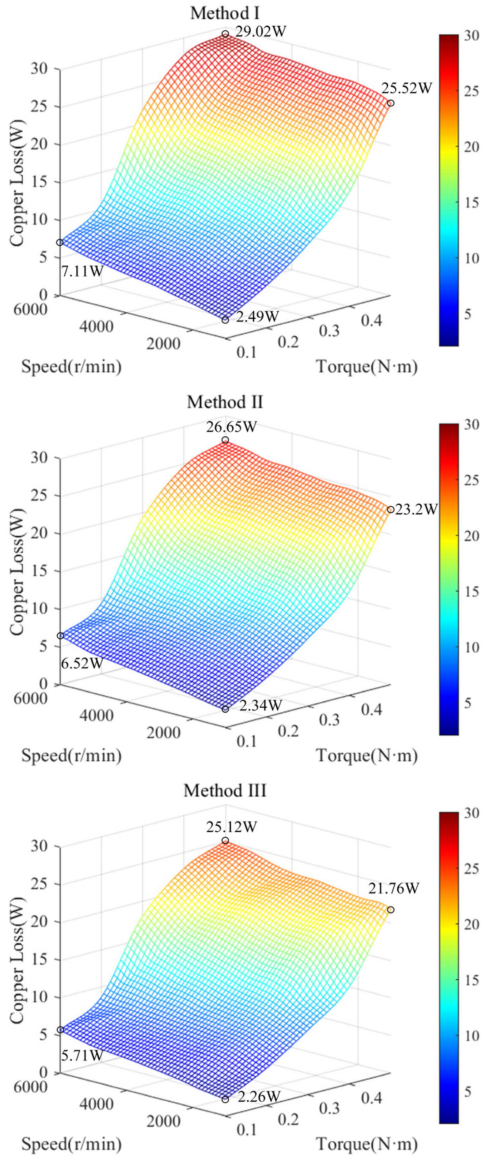

Fig. 13. Copper losses of the PMSM with the three methods at varied operating point.

PMSM increases with the increased load torque and speed, while the effect of the load torque is more significant.

Similarly, the input power and the output power of the PMSM are recorded at these operating points. By subtracting the output power and copper loss from the input power, the sum of iron loss and friction loss of the PMSM with the three methods is obtained. For example, at the reference speed 6000 r/min with the load torque 0.5 N·m, Fig. 14 shows the sum loss of the proposed method is 31.85 W, which is lower than 35.77 W of Method I and 33.52 W of Method II. Namely, with the comparison of Method I and Method II, the sum of iron loss and friction loss with Method III is reduced by 10.96% and 4.98%, respectively. It can be inferred that the friction loss of this experiment platform with different control strategies is equivalent at the same speed. And the color bars are identical in these 3-D figures. Thus, the improved LMC strategy can

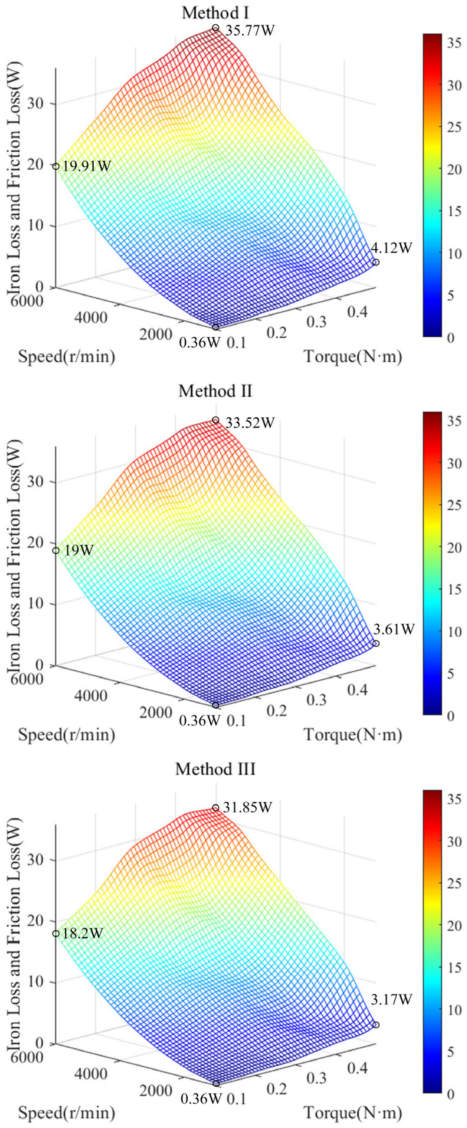

Fig. 14. Iron losses and friction loss of the PMSM with the three methods at varied operating point.

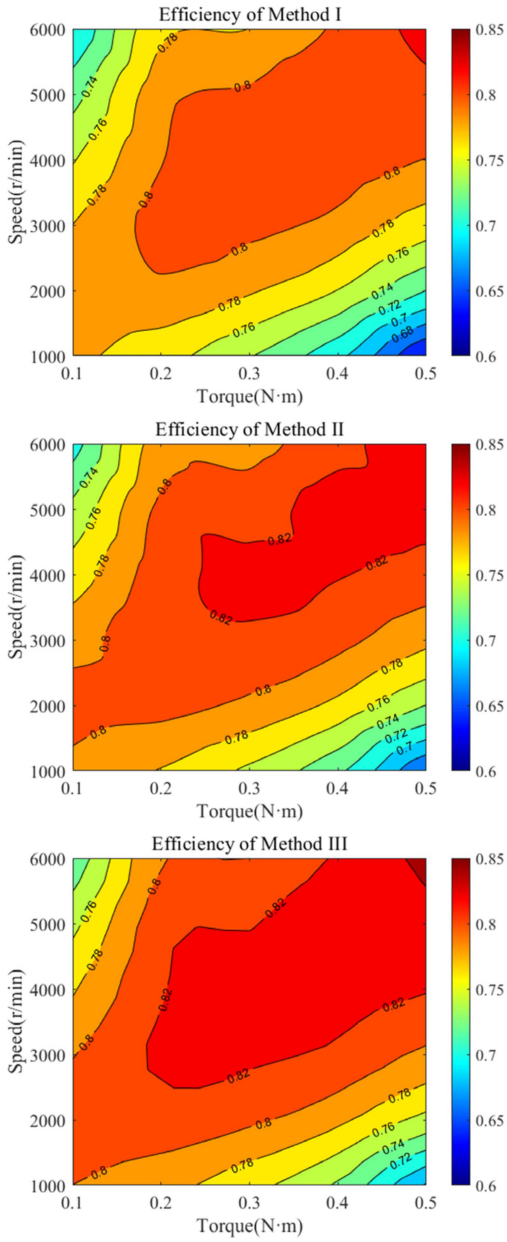

Fig. 15. Efficiency cloud maps of the PMSM with the three methods.

reduce the iron loss of the PMSM, and its effectiveness is better than traditional LMC strategy. In addition, it is possible to conclude that the iron loss is greatly affected by the speed of PMSMs.

The efficiency cloud maps of the PMSM with the three methods at varied operating point are shown in Fig. 15. The color bars in the three efficiency cloud maps are identical. For example, at the reference speed 6000 r/min with the load torque 0.5 N·m, the efficiency of the PMSM with Method III is about 84.65% which is higher than 82.90% of Method I and 83.93% of Method II. Similarly, at the other same operating points, the efficiency of Method II is higher than that of Method I, while the efficiency of Method III is higher than that of Method II. Therefore, the improved LMC strategy can increase the efficiency of PMSMs significantly which further verifies its effectiveness.

V. Conclusion

This article proposed an improved LMC strategy based on bivariate extreme value theory for PMSMs. First of all, based on the equivalent model of PMSMs considering both copper loss and iron loss, the electrical loss is derived as a function of d-q-axis current. Then, the optimal d-q-axis current is obtained by bivariate extreme value theory. Combined with the current equation in steady state, the optimal d-axis active current model is modeled. Meanwhile, the q-axis active current is obtained by the speed controller, so that the improved LMC strategy with implicit torque constraint is realized. In addition, a novel feedforward decoupling control module is added to the current controller to compensate the voltage drop on the R_s caused by the iron loss currents. Finally, compared with $i_d = 0$ control

method and traditional LMC strategy, the copper loss with the improved LMC strategy is reduced by 13.44% and 5.74%, and the sum of iron loss and friction loss is reduced by 10.96% and 4.98%, respectively. Therefore, the proposed LMC method can significantly reduce the electrical loss of PMSMs.

In addition, the improved LMC method is sensitive to the parameters of PMSMs, such as the stator resistance, stator inductance, iron loss resistance, and flux linkage, which are affected by temperature. Hence, to minimize the electrical loss of PMSMs at different temperature, the parameter identification is essential.

REFERENCES

[1] W. Huang, B. Du, T. Li, Y. Sun, Y. Cheng, and S. Cui, "Interturn short-circuit fault diagnosis of interior permanent magnet synchronous motor for electric vehicle based on search coil," *IEEE Trans. Power Electron.*, vol. 38, no. 2, pp. 2506–2515, Feb. 2023.

[2] Z. Zhang, Q. Sun, and Q. Zhang, "A computationally efficient model predictive control method for dual three-phase PMSM of electric vehicle with fixed switching frequency," *IEEE Trans. Ind. Appl.*, early access, doi: 10.1109/TIA.2023.3278255.

[3] M. Alzayed, H. Chaoui, and Y. Farajpour, "Dynamic direct voltage MTPA current sensorless drives for interior PMSM-based electric vehicles," *IEEE Trans. Veh. Technol.*, vol. 72, no. 3, pp. 3175–3185, Mar. 2023.

[4] M. N. Uddin and N. Patel, "Maximum power point tracking control of IPMSG incorporating loss minimization and speed sensorless schemes for wind energy system," *IEEE Trans. Ind. Appl.*, vol. 52, no. 2, pp. 1902–1912, Mar./Apr. 2016.

[5] H. Zhang, M. Dou, and J. Deng, "Loss-minimization strategy of nonsinusoidal back EMF PMSM in multiple synchronous reference frames," *IEEE Trans. Power Electron.*, vol. 35, no. 8, pp. 8335–8346, Aug. 2020.

[6] G. Feng, C. Lai, and N. C. Kar, "Speed harmonic based decoupled torque ripple minimization control for permanent magnet synchronous machine with minimized loss," *IEEE Trans. Energy Convers.*, vol. 35, no. 4, pp. 1796–1805, Dec. 2020.

[7] M. Sun, Y. Xu, and K. Han, "Structure and optimization design of cup winding permanent magnet synchronous machine in flywheel energy storage system," *IEEE Trans. Magn.*, vol. 59, no. 5, May 2023, Art. no. 8100805.

[8] H.-W. Jun, J.-W. Lee, G.-H. Yoon, and J. Lee, "Optimal design of the PMSM retaining plate with 3-D barrier structure and eddy-current loss-reduction effect," *IEEE Trans. Ind. Electron.*, vol. 65, no. 2, pp. 1808–1818, Feb. 2018.

[9] N. Denis, M. Inoue, K. Fujisaki, H. Itabashi, and T. Yano, "Iron loss reduction in permanent magnet synchronous motor by using stator core made of nanocrystalline magnetic material," *IEEE Trans. Magn.*, vol. 53, no. 11, Nov. 2017, Art. no. 8110006.

[10] W. Tong, S. Dai, S. Wu, and R. Tang, "Performance comparison between an amorphous metal PMSM and a silicon steel PMSM," *IEEE Trans. Magn.*, vol. 55, no. 6, Jun. 2019, Art. no. 8102705.

[11] H. A. G. Al-Kaf, S. S. Hakami, and K.-B. Lee, "Hybrid current controller for permanent-magnet synchronous motors using robust switching techniques," *IEEE Trans. Power Electron.*, vol. 38, no. 3, pp. 3711–3724, Mar. 2023.

[12] C. Cavallaro, A. O. Di Tommaso, R. Miceli, A. Raciti, G. R. Galluzzo, and M. Trapanese, "Efficiency enhancement of permanent-magnet synchronous motor drives by online loss minimization approaches," *IEEE Trans. Ind. Electron.*, vol. 52, no. 4, pp. 1153–1160, Aug. 2005.

[13] J. Lee, K. Nam, S. Choi, and S. Kwon, "Loss-minimizing control of PMSM with the use of polynomial approximations," *IEEE Trans. Power Electron.*, vol. 24, no. 4, pp. 1071–1082, Apr. 2009.

[14] W. Xie, X. Wang, F. Wang, W. Xu, R. Kennel, and D. Gerling, "Dynamic loss minimization of finite control set-model predictive torque control for electric drive system," *IEEE Trans. Power Electron.*, vol. 31, no. 1, pp. 849–860, Jan. 2016.

[15] H. M. Flieh, R. D. Lorenz, E. Totoki, S. Yamaguchi, and Y. Nakamura, "Dynamic loss minimizing control of a permanent magnet servomotor operating even at the voltage limit when using deadbeat-direct torque and flux control," *IEEE Trans. Ind. Appl.*, vol. 55, no. 3, pp. 2710–2720, May/Jun. 2019.

[16] Y. Shi, B. Sarlioglu, and R. Lorenz, "Real-time loss minimizing control of induction machines for dynamic load profiles under deadbeat-direct torque and flux control," *IEEE Trans. Ind. Appl.*, vol. 57, no. 4, pp. 3754–3762, Jul./Aug. 2021.

[17] Z. Xia et al., "Computation-efficient online optimal tracking method for permanent magnet synchronous machine drives for MTPA and flux-weakening operations," *IEEE J. Emerg. Sel. Topics Power Electron.*, vol. 9, no. 5, pp. 5341–5353, Oct. 2021.

[18] K. Huang, W. Peng, C. Lai, and G. Feng, "Efficient maximum torque per ampere (MTPA) control of interior PMSM using sparse Bayesian based offline data-driven model with online magnet temperature compensation," *IEEE Trans. Power Electron.*, vol. 38, no. 4, pp. 5192–5203, Apr. 2023.

[19] C. Lee and I. G. Jang, "Topology optimization of the IPMSMs considering both the MTPA and FW controls under the voltage and current limitations," *IEEE Trans. Ind. Electron.*, vol. 70, no. 8, pp. 8244–8253, Aug. 2023.

[20] E. S. Sergaki, P. S. Georgilakis, A. G. Kladas, and G. S. Stavrakakis, "Fuzzy logic based online electromagnetic loss minimization of permanent magnet synchronous motor drives," in *Proc. 18th Int. Conf. Elect. Mach.*, Sep. 2008, pp. 1–7.

[21] A. Balamurali, G. Feng, C. Lai, J. Tjong, and N. C. Kar, "Maximum efficiency control of PMSM drives considering system losses using gradient descent algorithm based on DC power measurement," *IEEE Trans. Energy Convers.*, vol. 33, no. 4, pp. 2240–2249, Dec. 2018.

[22] Z. Chen, W. Li, X. Shu, J. Shen, Y. Zhang, and S. Shen, "Operation efficiency optimization for permanent magnet synchronous motor based on improved particle swarm optimization," *IEEE Access*, vol. 9, pp. 777–788, 2021.

[23] J. Hang, H. Wu, S. Ding, Y. Huang, and W. Hua, "Improved loss minimization control for IPMSM using equivalent conversion method," *IEEE Trans. Power Electron.*, vol. 36, no. 2, pp. 1931–1940, Feb. 2021.

[24] M. N. Uddin, H. Zou, and F. Azevedo, "Online loss-minimization-based adaptive flux observer for direct torque and flux control of PMSM drive," *IEEE Trans. Ind. Appl.*, vol. 52, no. 1, pp. 425–431, Jan./Feb. 2016.

[25] M. N. Uddin, M. M. Rahman, B. Patel, and B. Venkatesh, "Performance of a loss model based nonlinear controller for IPMSM drive incorporating parameter uncertainties," *IEEE Trans. Power Electron.*, vol. 34, no. 6, pp. 5684–5696, Jun. 2019.

[26] N. Urasaki, T. Senjyu, and K. Uezato, "A novel calculation method for iron loss resistance suitable in modeling permanent-magnet synchronous motors," *IEEE Trans. Energy Convers.*, vol. 18, no. 1, pp. 41–47, Mar. 2003.

[27] R. Ni, D. Xu, G. Wang, L. Ding, G. Zhang, and L. Qu, "Maximum efficiency per ampere control of permanent-magnet synchronous machines," *IEEE Trans. Ind. Electron.*, vol. 62, no. 4, pp. 2135–2143, Apr. 2015.

[28] G. Liu, M. Liu, Y. Zhang, H. Wang, and C. Gerada, "High-speed permanent magnet synchronous motor iron loss calculation method considering multiphysics factors," *IEEE Trans. Ind. Electron.*, vol. 67, no. 7, pp. 5360–5368, Jul. 2020.

[29] J. Kim, I. Jeong, K. Nam, J. Yang, and T. Hwang, "Sensorless control of PMSM in a high-speed region considering iron loss," *IEEE Trans. Ind. Electron.*, vol. 62, no. 10, pp. 6151–6159, Oct. 2015.

[30] V. Ruuskanen, J. Nerg, M. Rilla, and J. Pyrhonen, "Iron loss analysis of the permanent-magnet synchronous machine based on finite-element analysis over the electrical vehicle drive cycle," *IEEE Trans. Ind. Electron.*, vol. 63, no. 7, pp. 4129–4136, Jul. 2016.

Zhuang Liu received the B.S. degree in electrical engineering and automation from Qingdao University, Qingdao, China, in 2018, and the M.S. degree in electrical engineering in 2021 from Beihang University, Beijing, China, where he is currently working toward the Ph.D. degree in electronic information with the School of Instrumentation Science and Optoelectronics Engineering and Astronautics.

His research interests include power electronics and high-speed permanent magnet motor control.

Kun Mao (Member, IEEE) received the B.S. degree in automation from the Southwest University of Science and Technology, Mianyang, China, in 2009, and the Ph.D. degree in precision instruments and machinery from Beihang University, Beijing, China, in 2018.

He is currently a Research Member with the School of Instrumentation Science and Optoelectronics Engineering, Beihang University. His research interests include power electronics and high-speed permanent magnet motor control.

Xusheng Lei was born in Henan, China, in 1977. He received the B.S. degree in automation from Zhengzhou University, Zhengzhou, China, in 1998, the M.S. degree in mechanical manufacturing and automation from Henan University of Science and Technology, Luoyang, China, in 2002, and the Ph.D. degree in control theory and control engineering from Shanghai Jiaotong University, Shanghai, China, in 2006.

He is currently a Professor with the School of Instrumentation Science and Optoelectronics Engineering, Beihang University, Beijing, China. His main research interests include high-performance control for small unmanned aerial vehicles and intelligent control for inertial stable platforms.

Shiqiang Zheng (Member, IEEE) was born in Shandong, China, in 1981. He received the Ph.D. degree in electrical and electronics engineering from Beihang University, Beijing, China, in 2011.

He is currently a Professor with the School of Instrumentation and Optoelectronic Engineering, Beihang University. He has been a Visiting Scholar with the Advanced Robotics Center, National University of Singapore, Singapore. His research interests include the magnetic bearing technologies in high-speed rotating machineries and attitude control actuators of spacecraft.

Haifeng Zhang received the M.S. degree in instrument and meter engineering and Ph.D. degree in precision instruments and machinery from Beihang University, Beijing, China, in 2016 and 2020, respectively.

He is currently a Research Member with the Key Laboratory of Ultra-Weak Magnetic Field Measurement Technology, Ministry of Education, School of Instrumentation and Optoelectronic Engineering, Beihang University, where he is also with Ningbo Institute of Technology and Beijing Engineering Research Center of High-Speed Magnetically Suspended Motor Technology and Application. His research interests include permanent magnet motor control, power electronics, magnetic shielding, and active magnetic compensation technology.